Int. J. Electrochem. Sci., 12 **(2017)** 7351 – 7364, doi: 10.20964/2017.08.09

International Journal of ELECTROCHEMICAL SCIENCE
www.electrochemsci.org

Computational Fluid Dynamic Simulations of Single-Phase Flow in a Spacer-Filled Channel of a Filter-Press Electrolyzer

Locksley Castañeda[1], *René Antaño*[1], *Fernando F. Rivera*[1], *José L. Nava*[2,*]

[1] Centro de Investigación y Desarrollo Tecnológico en Electroquímica, Parque Tecnológico Querétaro, Sanfandila, Pedro Escobedo, C.P. 76703 Querétaro, México.
[2] Universidad de Guanajuato, Departamento de Ingeniería Geomática e Hidráulica, Av. Juárez 77, Zona Centro, C.P. 36000, Guanajuato, Guanajuato, Mexico.
[*]E-mail: jlnm@ugto.mx

Received: 27 March 2017 / *Accepted:* 19 May 2017 / *Published:* 12 July 2017

Computational fluid dynamic (CFD) simulations were performed for single-phase flow in a spacer-filled channel of a filter-press electrolyzer solving the Reynolds-averaged Navier-Stokes (RANS) equations with the *k-ε* turbulence model. For the first time the physical presence of a turbulence promoter in a pre-pilot scale filter-press electrolyzer was included in the simulation, obtaining excellent agreement of simulations with experimental residence time distribution (RTD) results. CFD simulations evidence that net-like spacer homogenizes the flow distribution, provoking an increase in local Reynolds numbers. Also, the velocity profiles are strongly affected by the flow distributor at the inlet of the electrolyzer, but these become more uniform in the presence of the turbulence promoter.

Keywords: Flow hydrodynamics, Filter-press electrolyzer, Turbulence promoter, Turbulent flow

1. INTRODUCTION

Filter-press-type electrochemical reactors are commonly used in laboratory and industrial applications [1]. The operation of membrane electro-assisted processes, such as electrodialysis, salt splitting, energy storage, and electrosynthesis (e.g. Chlor-alkali synthesis), among other applications, is associated with the supply, removal and distribution of process electrolytes [1]. The performance of these technologies strongly depends on the uniformity of their fluid distribution both between individual working chambers and also over a working membrane surface [2]. In order to homogenize the fluid pattern, the net-like spacer or turbulence promoter is integrated between individual working chambers. The presence of a spacer disrupts the fluid and mixes the solution, which results in the

destabilization of the hydrodynamic boundary layer and enhances the mass transfer rate [1-5]. In addition, this turbulence promoter impedes the breaking of the membranes for possible changes in pressure between the individual working chambers and prevents direct contact between membranes and electrodes. It is important to highlight that the turbulence promoter increases the pressure drop, although mass transport enhancement often compensates these shortcomings [5].

Recently, several papers on systems filled with net-like spacers try to understand the transport phenomena obtained from experimental studies, by means of mathematical modeling based on computational fluid dynamics (CFD) techniques [2-4, 6]. For its robustness, reliability, and efficiency CFD techniques have been used to effectively study net-like spacer-filled channel geometry to optimize net-like spacers [2-4, 6].

In spite of several papers found in the literature regarding the non-ideal flow analysis of different turbulence promoters (net-like spacers), which are orientated to several physicochemical systems, it seems that reports on electrochemical systems are scarce. For example, Fimbres and Wiley [3] model a non-woven cylindrical filament spacer mesh in 3D and 2D using a periodic unit cell approach and apply a fully-developed mass fraction profile as the boundary condition for the solute. The 3D geometries were modeled solving the Navier-Stokes (NS) equations and showed greater mass transfer enhancement than that obtained in 2D, owing to 3D effects such as the occurrence of streamwise vortices, open spanwise vortices, and higher wall shear stresses perpendicular to the bulk flow. On the other hand, Picioreanu et al. [4] developed CFD simulations solving the NS equations in 3D of a 3×5 domain of feed spacer frames, highlighting the appearance of a heterogeneous flow pattern and the formation of preferential flow channels. Other simplified models in 2D have been tested to save computational resources. For example, Panek et al. [2] developed a 2D mathematical model of the flow hydrodynamics in a flat channel filled with a net-like spacer solving the NS equations at low and high Reynolds values where they analyze the convenience of neglecting flow inertia in the model. On the other hand, Ranade and Kumar [7] performed several simulations of different kinds of spacers in a rectangular “unit cell” solving the Reynolds-averaged Navier-Stokes (RANS) equations in 3D, while highlighting the CFD simulations of curvilinear spacers. Fimbres-Weihs and Wiley [6] reviewed the CFD simulation of different kinds of spacer-filled channel geometries and net-like spacer filaments in a flow pattern in the scale of few centimeters long emphasizing that in the past decade, many 2D flow studies employing CFD have been published and more recently 3D solutions are slowly emerging.

In divided filter-press electrolyzers with parallel plate electrodes at pilot scale, turbulence promoters have been used to improve mass transport [1]. In this regard, several experimental studies of mass transport showing the influence of different net plastic arrangements have been reported (in pre-pilot scale), highlighting that these turbulence promoters enhance mass transport by a factor of two to twelve [5, 8]. Moreover, non-ideal flow analysis with turbulence promoters inside filter-press electrolyzers have only been performed by parametric models which took into account the experimentally obtained dispersion model [9-13]; in empty channels CFD attempts are ample [14-22]. Modeling the fluid hydrodynamics inside individual net-like spacer-filled channel of filter-press type electrolyzers is essential to guaranteeing the acceptable fluid environment, mass transport, and current distribution during scaling-up.

The novelty of this communication focuses on CFD simulations in a turbulence promoter-filled channel of a well-engineered filter-press type electrolyzer (in pre-pilot scale) solving the RANS equations with the k–ε turbulence model. To our understanding, this is the first time that a CFD simulation considers, with success, the physical presence of a turbulence promoter. A typical polypropylene net-like spacer (turbulence promoter type-D) was employed [1]. RTD was obtained solving the averaged diffusion-convection equation. Simulations were validated with experimental flow visualizations and RTD.

2. DESCRIPTION OF THE FM01-LC

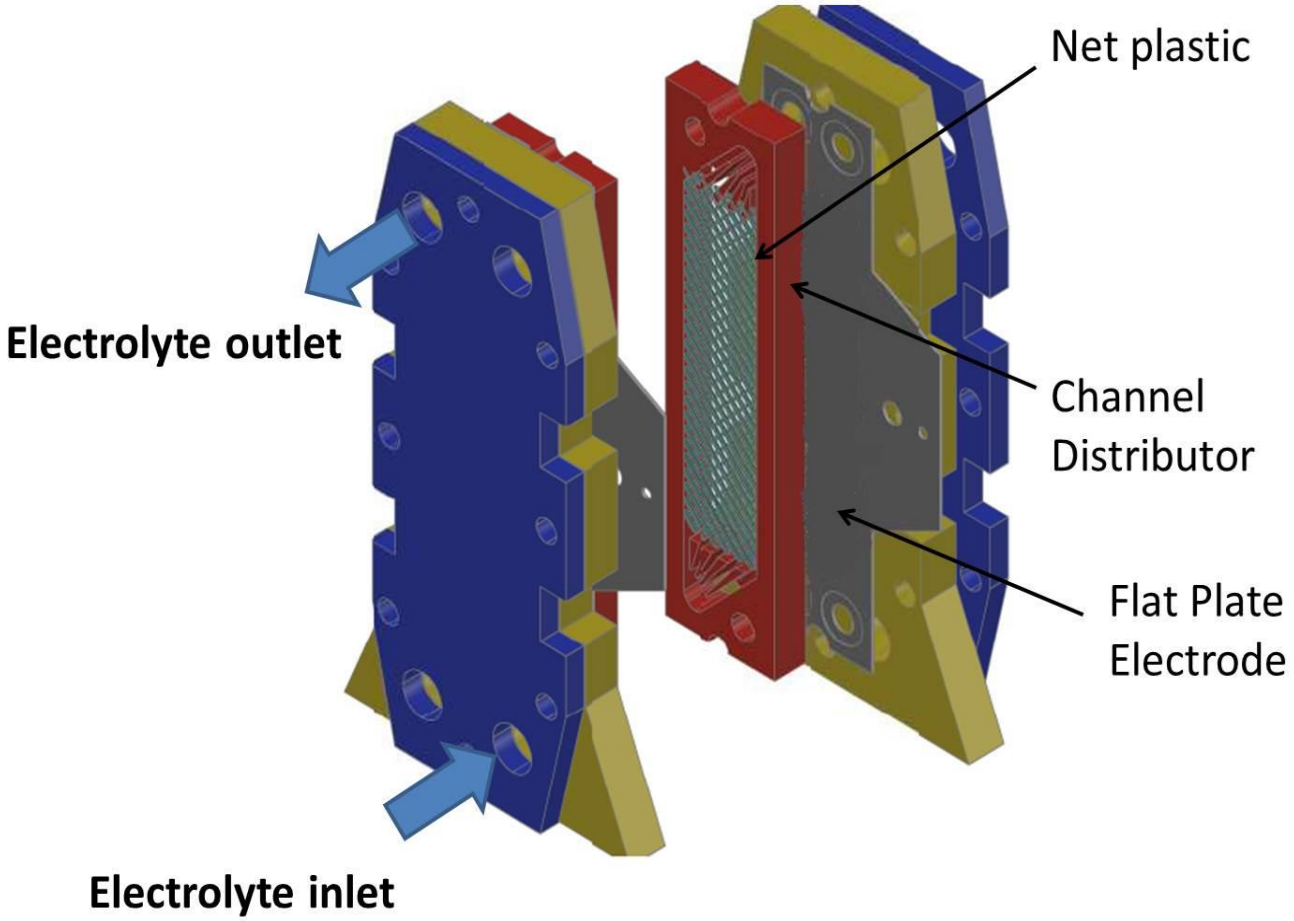

Figure 1. Exploded view of the FM01-LC pre-pilot electrolyzer including the net-like spacer (turbulence promoter type D).

Fig. 1 shows a scheme of the FM01-LC filter press reactor. Fig. 2 shows the simulation domain used as a basis for the computational analysis. The dimensions of the flow cell are showed in the Table 1. The inset of Fig. 2 shows the geometry of turbulence promoter type D.

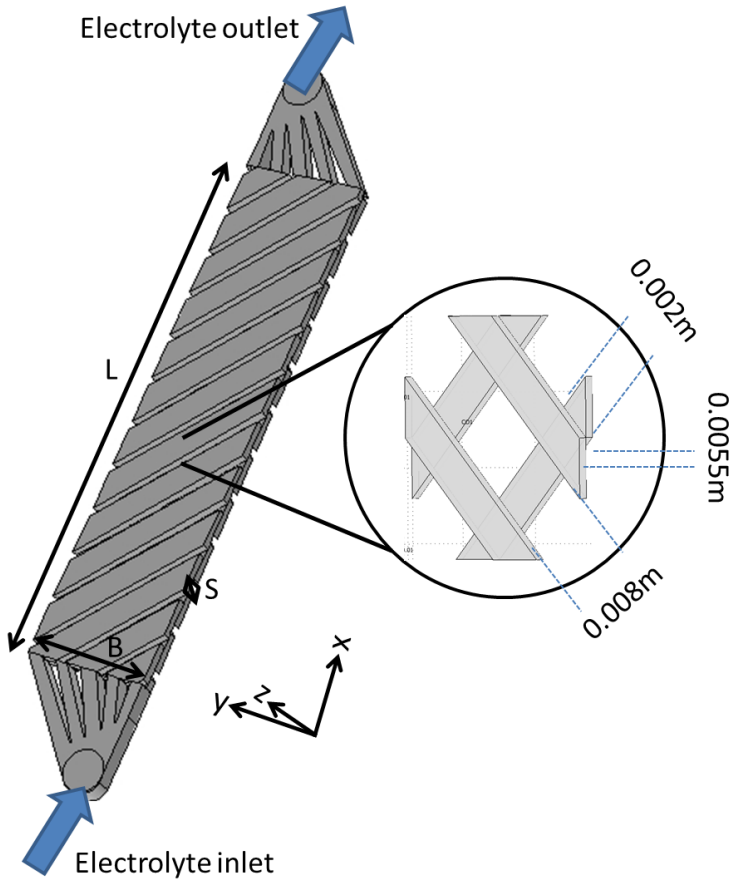

Figure 2. Simulation domain established to implement the CFD simulation. The inset enlarges the turbulence promoter.

Table 1. Electrode dimensions and details on the FM01-LC electrolyzer

Electrode length, *L*	0.16 m
Electrode height, *B*	0.04 m
Electrode spacing, *S*	0.0055 m
Electrode area, *A*	0.0064 m^2
Hydraulic (equivalent) diameter, $d_e = 2BS/(B + S)$	0.0097 m
Turbulence promoter	Plastic mesh type D *CD and **LD = 11 mm.
Overall voidage, ε	0.83

* CD = internal dimension of shorter diagonal mesh.

**LD = internal dimension of longer diagonal mesh.

Overall voidage is the ratio of the free space in the channel to overall channel volume.

3. FORMULATION OF NUMERICAL SIMULATION.

The mean linear flow rates studied here were comprised between (0.038–0.15 m s^{-1}) giving Reynolds numbers between 300–1500, characteristic of a laminar flow. However, because the

turbulence promoter provokes high velocity streams causing 3D flow instabilities and eddy formation, we solve the RANS and the averaged diffusion-convection equations for the CFD visualizations and theoretical RTD determinations.

3.1. Turbulent Flow

The RANS and continuity equations are applied:

$$\rho(\boldsymbol{u}\cdot\nabla)\boldsymbol{u} = -\nabla P + \nabla\cdot\left((\mu+\mu_T)(\nabla\cdot\boldsymbol{u}+(\nabla\cdot\boldsymbol{u})^T)\right) \quad (1)$$

$$\nabla\cdot(\rho\boldsymbol{u}) = 0 \quad (2)$$

Where μ denotes the dynamic viscosity of the fluid, $\boldsymbol{u}$ is the velocity vector, P is the pressure, ρ is the density of the fluid, where the so-called Reynolds stresses can be expressed in terms of a turbulent viscosity μ_T, according to the standard k–ε turbulence model:

$$\mu_T = \rho C_\mu \frac{k^2}{\varepsilon} \quad (3)$$

$$\rho(\boldsymbol{u}\cdot\nabla)k = \nabla\cdot\left(\left(\mu+\frac{\mu_T}{\sigma_k}\right)\nabla k\right) + P_k - \rho\varepsilon \quad (4)$$

$$\rho\boldsymbol{u}\cdot\nabla\varepsilon = \nabla\cdot\left(\left(\mu+\frac{\mu_T}{\sigma_\varepsilon}\right)\nabla\varepsilon\right) + C_{e1}\frac{\varepsilon}{\kappa}P_k - C_{e2}\rho\frac{\varepsilon^2}{k} \quad (5)$$

Where k is the turbulent kinetic energy, ε is the turbulent energy dissipation rate, P_k is the energy production term ($P_k = \mu_T[\nabla\boldsymbol{u}:(\nabla\boldsymbol{u}+(\nabla\boldsymbol{u})^T]$), and C_μ (0.09), C_{e1} (1.44), C_{e2} (1.92), σ_k (1), σ_ε (1.3) are dimensionless constant values that are obtained by data fitting for a wide range of turbulent flows [23-24]. The notation $(\ )^T$ refers to the transpose of $\nabla\boldsymbol{u}$, and it should not be confused with any turbulent suffix.

This model is applicable at high Reynolds numbers. The wall functions are usually used as boundary condition. These functions are based on a universal velocity distribution, which in a turbulent layer is described by the following equation:

$$u^+ = 2.5\ln y^+ + 5.5 \quad (6)$$

Where u^+ is the normalized velocity component inside the logarithmic boundary layer, and y^+ is the dimensionless distance from the wall, $y^+ = \rho u_\tau y/\mu$, where u_τ is the friction velocity, $u_\tau = C_\mu^{1/4}\sqrt{k}$ and y is the thickness from the wall [24].

To solve equations (1)-(5), the corresponding boundary conditions are as follows:

1) A normal inflow velocity at the inlet, $\boldsymbol{u} = -\boldsymbol{n}U_0$, an initial turbulent kinetic energy, k=

k_0; and an initial energy dissipation rate $\varepsilon=\varepsilon_0$. Where $\boldsymbol{n}$ is the unit normal vector, U_0 is the inflow velocity.

2) A normal stress equal to a pressure at the outlet, $\left[-P+\left(\mu+\mu_T\right)\left(\nabla \boldsymbol{u}+(\nabla \boldsymbol{u})^T\right)\right]\boldsymbol{n}=-\boldsymbol{n}P_0$, with $\nabla\varepsilon\cdot\boldsymbol{n}=0$; and $\nabla k\cdot\boldsymbol{n}=0$, where P_0 is the pressure at the cell exit of the cell. This last equation expresses that the turbulent characteristic of whatever is outside the computational domain is guided by the flow inside the computational domain [25]. Such an assumption is physically reasonable as long as relatively small amounts of fluid enter the system [20].

3) A velocity u^+ given by equation (6) at a distance y^+ from a solid surface, for all other boundaries.

The value of y^+ was fixed at 11.1. This value is in the fully turbulent region ($y^+ > 10$), where the turbulent stresses and fluxes are more important [26]. The values of k_0 and ε_0 were fixed at values of 0.005 $m^2\ s^{-2}$ and 0.005 $m^2\ s^{-3}$, these values are commonly used for incompressible flows in pipes and channels [24].

3.2 Tracer Simulation in the turbulence promoter-filled channel

The averaged diffusion-convection equation, analogous to the RANS equation, was employed to model the tracer inside the spacer-filled channel:

$$\frac{\partial c}{\partial t}=\nabla\cdot\left(D_i+D_{i,t}\right)\nabla c+\boldsymbol{u}\cdot\nabla c \qquad (7)$$

Where $\boldsymbol{u}$ was the averaged velocity vector (determined from Eq. (1, 2), c is the averaged concentration, D_i is the diffusion coefficient and $D_{i,T}$ is the eddy diffusivity or turbulent diffusivity. Eddy diffusivity can be determined from the turbulent Schmidt number ($Sc_T=\mu_T/(\rho D_{i,T})$) described by the following Kays–Crawford model [17-18]:

$$Sc_T=\left(\frac{1}{2Sc_{T\infty}}+\frac{0.3}{\sqrt{Sc_{T\infty}}}\frac{\mu_T}{\rho D_i}-\left(0.3\frac{\mu_T}{\rho D_i}\right)\left(1-exp\left(-\frac{\rho D_i}{0.3\mu_T\sqrt{Sc_{T\infty}}}\right)\right)\right)^{-1} \qquad (8)$$

Where $Sc_{T\infty}$ = 0.85.

Considering perfect mixing conditions before the inlet and after the outlet of the reactor, the boundary and the initial conditions established are as follows:

- Before tracer injection in the reactor (t = 0), the tracer concentration is zero, c = 0. To simulate the tracer pulse injection, normally a short time concentration pulses in the form of triangle, square, delta Dirac or Gaussian functions are used. Numerically it is complicated to find a correct function that exactly represents the experimental pulse, causing variations in the RTD prediction [27,

28]. In this paper, we employed a Gaussian pulse function: $y(t) = \frac{1}{\sigma\sqrt{2\pi}} e^{\frac{-(t-t=0)^2}{2\sigma^2}}$, where σ is the standard deviation. Thus, at the inlet, $c = c_0 y(t)/y(0)$. Here, c_0 is the initial tracer concentration (Cu^{2+} 0.005 mol cm^{-3}). To simulate the tracer injection, the Gaussian pulse function time interval was varied from 3 to 4 s using a standard deviation from 1.5 to 2.7.

- At the electrolyte outlet, $\boldsymbol{n} \cdot (-(D + D_T)\nabla C + \boldsymbol{u} \cdot \nabla C) = 0$.
- For all other boundaries, $-\boldsymbol{n} \cdot N = 0$, where *N* is the flux of the tracer.

3.3 Simulation

Simulations in 3-D for laminar and turbulent flow inside the reactor were carried out in the simulation domain shown in Fig. 2, through the finite element method. The commercial software employed here was COMSOL Multiphysics® (4.4). Simulation domains of 124 261 mesh elements were considered. The wall roughness was assumed to have a negligible effect. Table 2 shows the electrolyte input properties for the simulations. The simulations were performed at four different inflow velocities U_0: 0.038, 0.075, 0.11, and 0.15 m s^{-1}.

Table 2. Electrolyte properties used in the numerical simulation of RTD at 293 K.

Global diffusion coefficient of Cu^{2+}, D (m^2 s^{-1})	5.4×10^{-10}
Initial concentration of Cu^{2+}, c_0 (mol m^{-3})	50
Dynamic viscosity, μ (gr m^{-1} s^{-1})	1

Eqs. (1)-(5) for turbulent flow were solved for all inflow velocities. The tracer simulation needed the solution of Eqs. (7-8), and the computational animations were performed and compared with experimental tracer visualizations.

The simulation of the normalized RTD curve, *E(t)*, which describes the tracer distribution in certain periods of time for the stream of fluid leaving the reactor can be assessed according to Eq. (9) [29]:

$$E(t) = \frac{c(t)}{\int_0^\infty c(t)dt} \quad (9)$$

Where *c(t)* is the time-dependent concentration response. Simulations of RTD curves in the spacer-filled channel was performed by taking the *c(t)* solution of the Eqs. (7). The solver employed was iterative, FGMRES, and a relative tolerance of accuracy of the CFD simulations considered a convergence criterion below 1×10^{-5}. A 64 bit desktop PC workstation with two Intel(R) Xeon(R) 2.30 GHz processors and 96 GB of RAM was used for computational work.

4. EXPERIMENTAL

4.1 Tracer visualization (TV)

In order to visualize experimental flow patterns inside the FM01-LC reactor 1 mL of colored tracer (food grade colorant Carmine 50 at concentration of 1 g L^{-1}) was injected at 1.5 cm before the FM01-LC inlet. To visualize the flow inside the channel of the filter-press electrolyzer, one of the sides of the reactor was replaced by a polycarbonate transparent plate. The tracer path was filmed using a digital camera of 720 pixels.

4.2. RTD

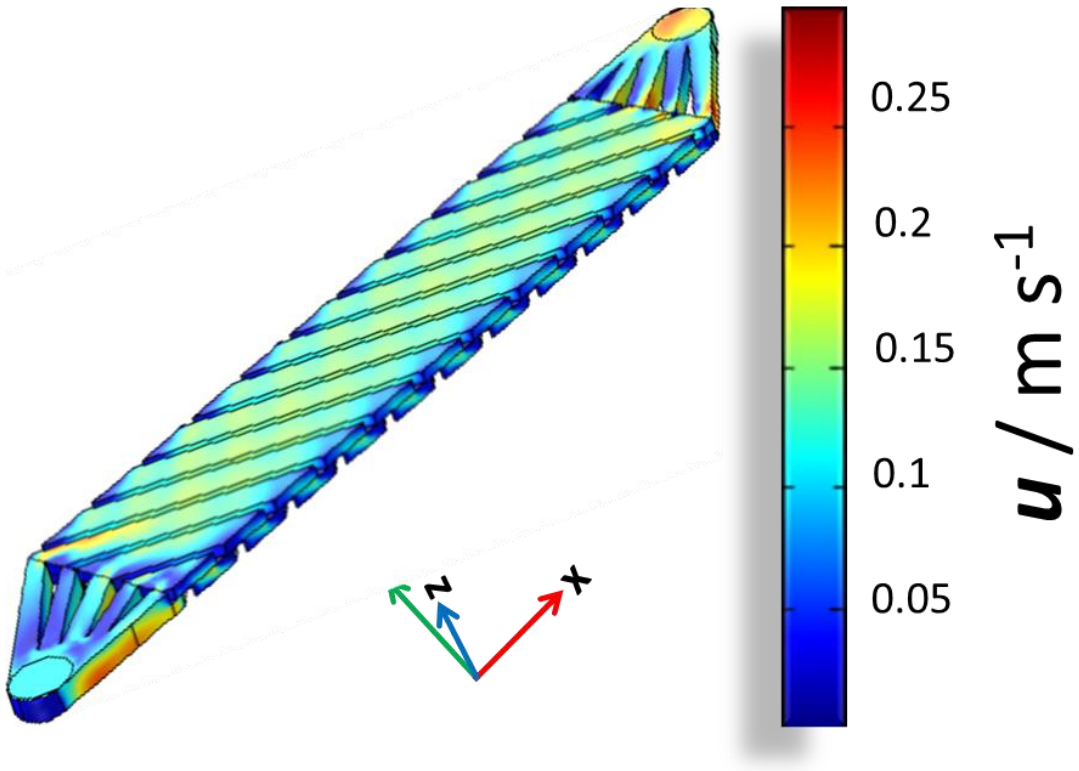

Figure 3. Simulated velocity field magnitude at characteristic inflow velocity of 0.11 m s^{-1}.

For RTD analysis the Carmin 50 tracer was not used owing to the low reproducibility of the colorimetric method. For this reason, an electrochemical method to perform RTD tests was implemented. Copper sulfate (1 mL of 0.05 M) was injected with a syringe at the inlet of the FM01-LC reactor. At the FM01-LC reactor exit, the Cu(II) ions were measured online by employing a typical two electrode cell arrangement using two copper wires as electrodes; the cupric ions were quantified by the typical transient current at a holding cell potential of -0.5 V and the current response was measured with the potentiostat-galvanostat. It is important to mention that at such cell potential, a limiting current of copper deposition governs the cathodic process, thereby ensuring that the response only depends on the cupric ion concentration. This quantification method is fast enough and very

sensitive to capture the rapid concentration changes at the reactor outlet [28]. The experimental RTD curve, *E(t)*, was constructed using the recorded time-dependent current intensity response *I(t)* at the exit of the reactor and by the use of Eq. (9) except that the *c(t)* is substituted by *I(t)*. The tracer tests were performed at different volumetric flow rates (*Q*): 0.1, 0.2, 0.3, 0.4, 0.8 L min^{-1}, giving inflow velocities of 0.038, 0.075, 0.11, and 0.15 m s^{-1}.

5. RESULTS AND DISCUSSION

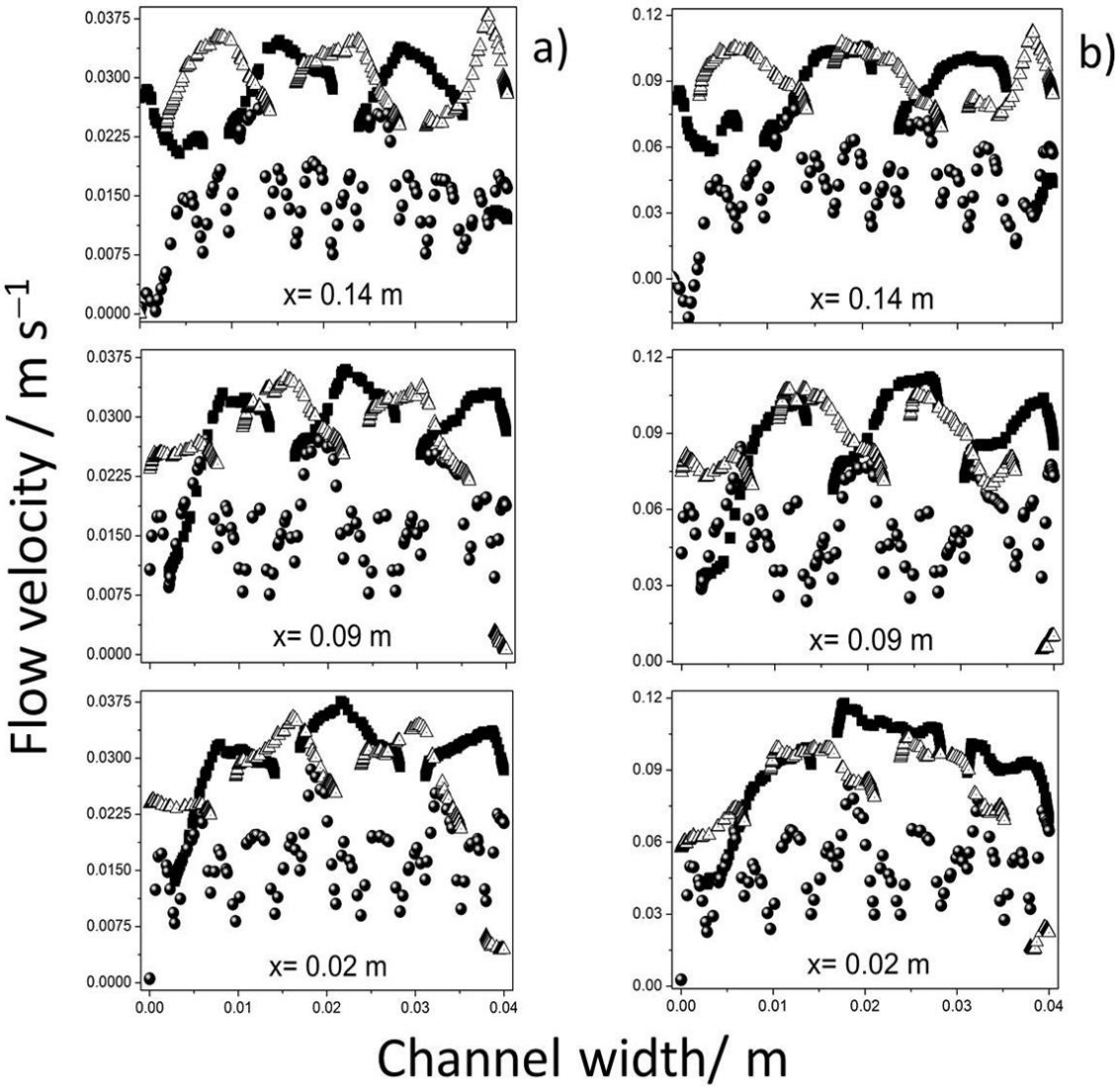

Figure 4. Simulated velocity profiles in the net-like spacer-filled channel at characteristic inflow velocities of: (a) 0.038 m s^{-1} and (b) 0.11 m s^{-1}, evaluated at three distances in *x*-coordinate (showed in the Figure) and at three thickness in z-coordinate: (■) 0.0014 m, (●) 0.0028 m, (▲) 0.0041 m.

Fig. 3 shows the velocity field plots for a characteristic influent velocity of 0.11 m s^{-1}, where it can be observed the effect of inlet flow distributor on the velocity, while net-like spacer modifies such velocity pattern throughout the channel. Figs. 4 (a) and (b) show the velocity profiles developed along

channel width (in the *y*–coordinate) obtained from the velocity field plots at inflow velocities of 0.038 and 0.11 m s^{-1}, respectively. These profiles were also determined at three different heights of 0.0014, 0.0028 and 0.0041 m in the *z*–coordinate, and at three different lengths in the *x*–coordinate. From the analysis of Fig. 4 a chaotic flow rate distribution in the channel width and all lengths (at *x*=0.02, 0.09, and 0.14 m) is observed, which is provoked by the net-like spacer.

The net-like spacer slightly provokes flow streams following disordered ways, as is expected in turbulent flow (Fig. 5 a), increasing local flow velocities and enhancing local Re values (Fig. 5 b). This behavior consequently enhances mass transport in parallel plate electrodes as was experimentally [5, 8] and theoretically demonstrated [30]. Similar CFD analyses were performed at inflow rates of 0.075 and 0.15 m s^{-1} (not shown herein), which developed similar flow patterns to that obtained at 0.038 and 0.11 m s^{-1}.

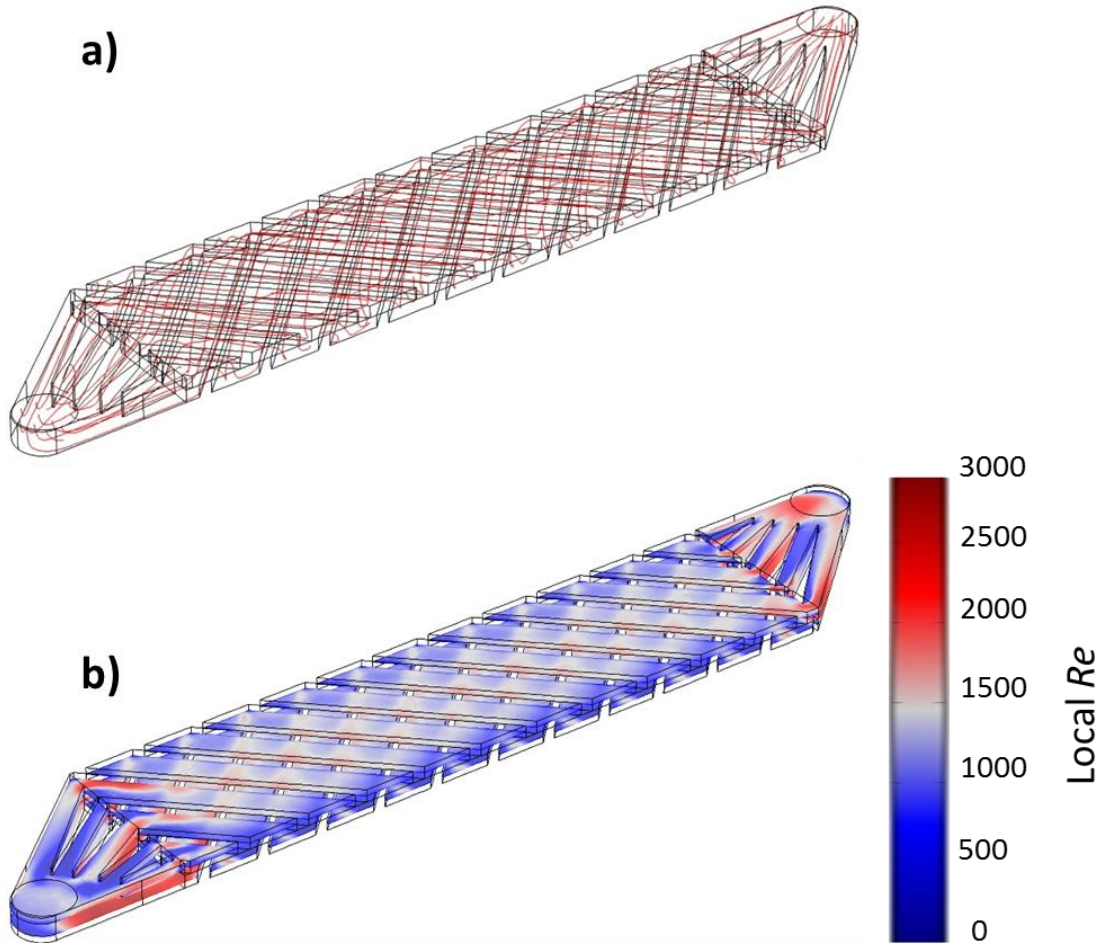

Figure 5. Streamlines plots (a) and Local Reynolds numbers (b) in the net-like spacer-filled channel at characteristic inflow velocity of 0.11 m s^{-1}. 100 streamlines was plotted, with starting and outlet points at the inlet and exit of the filter-press cell electrolyzer.

Fig. 6 shows the comparison of the experimental tracer visualization and its simulation along the channel with the turbulence promoter at characteristic inflow velocity of 0.11 m s^{-1}. A good qualitative similitude between theoretical and experimental tracer visualization is observed. It is

important to remark that the net-like spacer aligns the flow field. Similar tracer analysis performed at inflow rates of 0.038, 0.075 and 0.15 m s^{-1} (not shown herein) developed similar patterns to that obtained at 0.11 m s^{-1}.

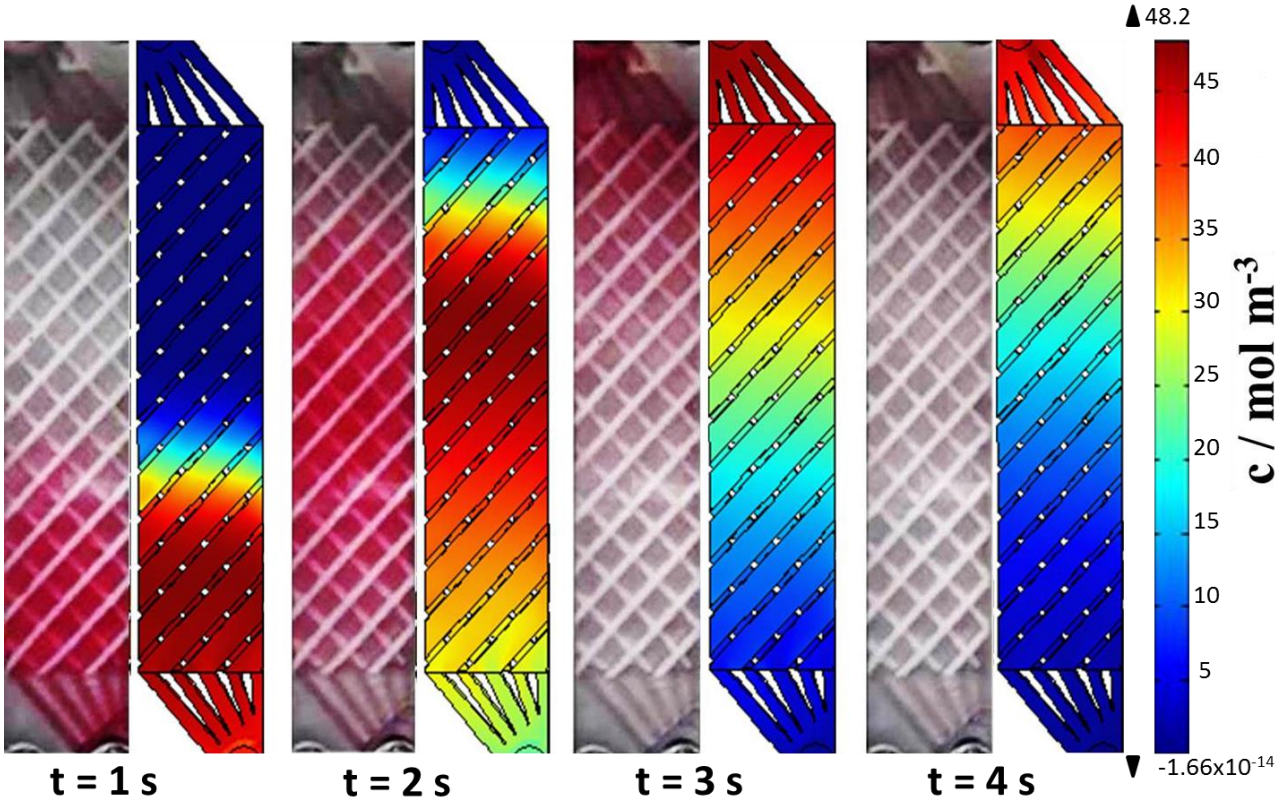

Figure 6. Comparisons of the tracer visualization between experimental and theoretical results at characteristic inflow velocity of 0.11 m s^{-1}.

In order to perform a quantitative analysis of the flow distributions, RTD simulations were validated with experimental data [31]. Fig. 7 shows excellent agreement between the experimental and simulated RTD in the channel with the turbulence (giving an error < 6%), at inflow velocities of 0.038, 0.075, 0.11 and 0.15 m s^{-1} (Reynolds number ($Re=U_0 d_e/\upsilon$) of 340, 728, 1067, and 1455), as a function of the dimensionless residence time (t/τ), where τ is the spatial residence time given by the ratio between the length of the FM01-LC and the inflow velocity ($\tau = L/U_0$). The shape of the simulated and experimental curves is similar and the maximum of the E-t/τ is close to unity, which is characteristic of a quasi-plug flow pattern. In addition, the RTD curves did not exhibit tailing at such *Re* values.

Comparisons of theoretical and experimental RTD curves and flow visualizations showed that the formulation of the numerical simulation proposed here is appropriate to reproduce the flow pattern inside the net-like spacer-filled channel of a filter press type electrolyzer and it can be used for further scaling-up studies.

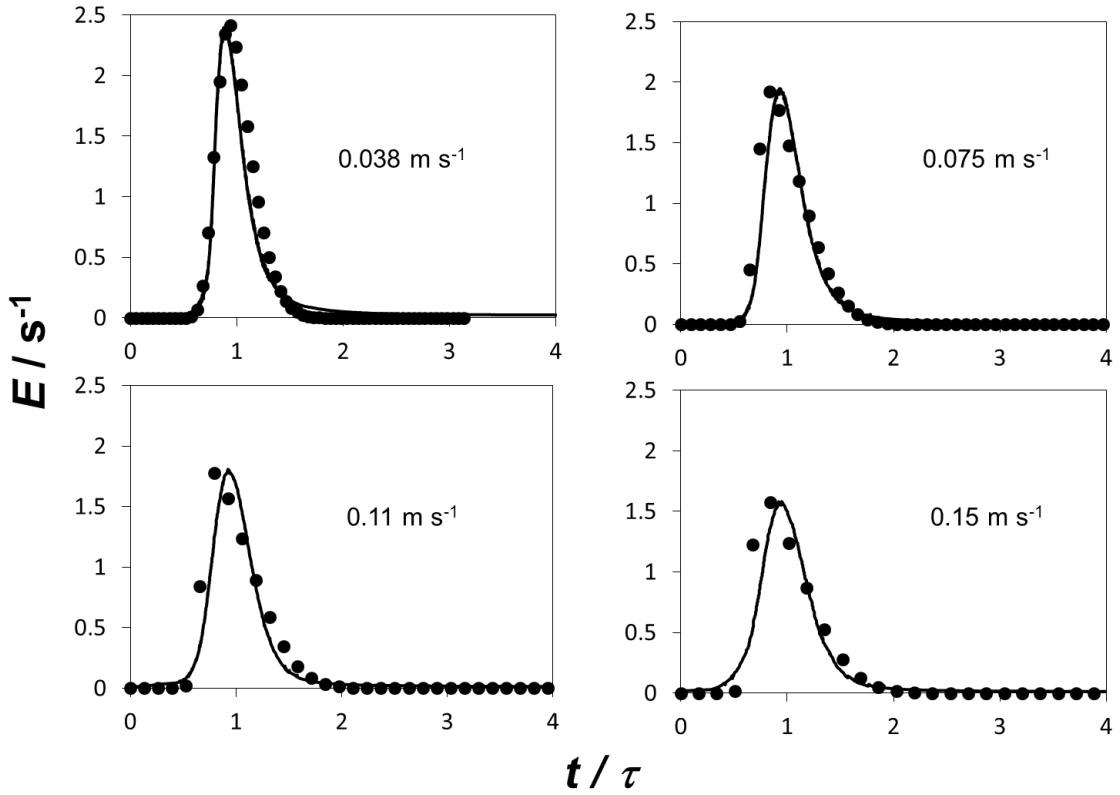

Figure 7. Comparison of experimental (—) and theoretical (•) RTD curves at different inflow velocities showed in the figure.

5. CONCLUSIONS

This work presented a way to analyze the hydrodynamic behavior of the net-like spacer-filled channel of a filter press type electrolyzer, solving the RANS equations. To our understanding, this is the first time that a CFD simulation considers, with success, the physical presence of a turbulence promoter. Theoretical RTD curves were obtained by solving the averaged diffusion-convection equation, taking into account the local velocity vectors obtained by the solution of RANS equations. Excellent agreement of simulations with experimental RTD was obtained. Turbulence promoter (type D) homogenizes the RTD for all flow rates studied here (0.038–0.15 m s^{-1}). This last is a desirable condition to guaranteeing the acceptable fluid environment, mass transport, and current distribution during scaling-up. The formulation of the numerical simulation model proposed here might be employed to design novel geometries of turbulence promoters and/or novel three-dimensional electrode shapes for their use in electrochemical reactors.

ACKNOWLEDGEMENTS
L.F. Castañeda would like to thank CONACYT for the scholarship No. 240492 granted. J.L. Nava gratefully acknowledges Universidad de Guanajuato for the financial support through the project No. 886/2016.

Symbols used

c	[mol m^{-3}]	Concentration of the tracer
D	[m^2 s^{-1}]	Diffusion coefficient
d_e	[m]	Equivalent diameter
$E(t)$	[s^{-1}]	Normalized RTD curve
$I(t)$	[A]	Time-dependent current intensity response
k	[m^2 s^{-2}]	Turbulent kinetic energy
L	[m]	Length of the cell
$\boldsymbol{n}$		Unit normal vector
N	[mol m^{-2} s^{-2}]	Flux of the tracer
P	[Pa]	Pressure
Q	[m^3 s^{-1}]	Volumetric flow rates
Re		Reynolds number
t	[s]	Time
$\boldsymbol{u}$	[m s^{-1}]	Velocity vector
υ	[m^2 s^{-1}]	Kinematic viscosity
y	[m]	Thickness from the wall

Greek Symbols

ε	[m^2 s^{-3}]	Turbulent energy dissipation rate
μ	[Kg m^{-1} s^{-1}]	Viscosity
ρ	[Kg m^{-3}]	Density
σ		Standard deviation
τ	[s]	Spatial residence time

Sub- and Superscripts

c_0	[mol m^{-3}]	Initial tracer concentration
C_μ		Dimensionless constant values
C_{e1}		Dimensionless constant values
C_{e2}		Dimensionless constant values
D_i	[m^2 s^{-1}]	Diffusion coefficient
$D_{i,T}$	[m^2 s^{-1}]	Eddy diffusivity or turbulent diffusivity
ε_0	[m^2 s^{-3}]	Initial energy dissipation rate
k_0	[m^2 s^{-2}]	Initial turbulent kinetic energy
μ_T	[Kg m^{-1} s^{-1}]	Turbulent viscosity
P_k		Energy production term
P_0	[atm]	Pressure at the exit of the cell
Sc_T		Turbulent Schmidt number
σ_k		Dimensionless constant values
σ_ε		Dimensionless constant values
U_0	[m s^{-1}]	Inflow velocity
u_τ	[m s^{-1}]	Friction velocity
u^+		Normalized velocity component
y^+		Dimensionless distance from the wall

Abbreviations

CFD	Computational Fluid Dynamic
NS	Navier-Stokes
RANS	Reynolds-averaged Navier-Stokes
RTD	Residence time distribution
TV	Tracer visualization

References

1. F.F. Rivera, C. Ponce de León, F.C. Walsh, J.L. Nava, *Electrochim. Acta.* 163 (2015) 338.
2. P. Pánek, R. Kodýum, D. Snita, K. Bouzek, *J. Membr. Sci*. 492 (2015) 588.
3. G.A. Fimbres, D.E. Wiley, *J. Membr. Sci.* 306 (2007) 228.
4. C. Picioreanu, J.S. Vrouwenvelder, M.C.M. Loosdrecht, *J. Membr. Sci.* 345 (2009) 340.
5. M. Griffiths, C. Ponce de León, F.C. Walsh, *AIChE J.* 51 (2005) 682.
6. G.A. Fimbres-Weihs, D.E. Wiley, *Chem. Eng. Process.* 49 (2010) 759.
7. V.V. Ranade, A. Kumar, *J. Membr. Sci.* 271 (2006) 1.
8. C.J. Brown, D. Pletcher, F.C. Walsh, J.K. Hammond, D. Robinson, *J. Appl. Electrochem.* 23 (1993) 38.
9. P. Trinidad, F.C. Walsh, *Electrochim. Acta.* 41 (1996) 493.
10. P. Trinidad, F.C. Walsh, C. Ponce de León, *Electrochim. Acta.* 52 (2006) 604.
11. F.F. Rivera, M.R. Cruz-Díaz, E.P. Rivero, I. González, *Electrochim. Acta.* 56 (2010) 361.
12. A.N. Colli, J.M. Bisang, *Electrochim. Acta.* 56 (2011) 7312.
13. A. Montillet, J. Comiti, J. Legrand, *J. Appl. Electrochem*. 23 (1993) 1045.
14. J.A. Delgadillo, R. Enciso, C. Ojeda, I. Rodríguez, *Int. J. Electrochem. Sci.* 7 (2012) 2065.
15. J.L.C. Santos, V. Geraldes, S. Velizarov, J.G. Crespo, *Chem. Eng. J.* 157 (2010) 379.
16. L. Vázquez, A. Alvarez-Gallegos, F.Z. Sierra, C. Ponce de León, F.C. Walsh, *Electrochim. Acta.* 55 (2010) 3437.
17. E.P. Rivero, F.F. Rivera, M.R. Cruz-Díaz, E. Mayen, I. González, *Chem. Eng. Res. Des*. 90 (2012) 1969.
18. E.P. Rivero, M.R. Cruz-Díaz, F.J. Almazán-Ruiz, I. González, *Chem. Eng. Res. Des*. 100 (2015**)** 422.
19. M.R. Cruz-Díaz, E.P. Rivero, F.J. Almazán-Ruiz, A.T. Mendoza, I. González, *Chem. Eng. Process*. 85 (2014) 145.
20. T. Pérez, C. Ponce de León, F.C. Walsh, J.L. Nava, *Electrochim. Acta*. 154 (2015) 352.
21. C. Bengoa, A. Montillet, P. Legentilhomme, J. Legrand, *Ind. Eng. Chem. Res*. 39 (2009) 2199.
22. J.A. Frías-Ferrer, I. Tudela, O. Louisnard, V. Sáez, M.D. Esclapez, M.I. Diez-García, P. Bonete, J. González-García, *Chem. Eng. J*. 169 (2011) 270.
23. P.S. Bernard, J.M. Wallace, *Turbulent Flow: Analysis, Measurement and Prediction*, (2002) John Wiley & Sons, New Jersey, USA.
24. H.K Versteeg, W. Malalasekera, *An Introduction to Computational Fluid Dynamics: The Finite Volume Method*, (1995) Prentice Hall, London.
25. D.C. Wilcox, *Turbulence Modeling for CFD*, (1998) DCW Industries Inc., California, USA.
26. H. Schlichting, *Boundary-Layer Theory*, (1979) MC Graw-Hill, New York, USA.
27. M.J. Rivera, M. Trujillo, V. Romero-García, J.A. López-Molina, E. Berjano, *Int. Commun. Heat Mass Transfer*. 46 (2013) 7.
28. M. Rosales, T. Pérez, J.L. Nava, *Electrochim. Acta.* 194 (2016) 338.
29. H.S. Fogler, *Elements of Chemical Reaction Engineering*, (2005) Prentice Hall, New Jersey, USA.
30. J. Lira-Teco, F. Rivera, O. Frías-Moguel, J. Torres-González, Y. Reyes, R. Antaño-López, G. Orozco, F. Castañeda-Zaldivar, *Fuel*. 167 (2016) 337.
31. J.C.G. Peres, U. De Silvio, A.C.S.C. Teixeira, R. Guardani, A.S Vianna Jr., *Chem. Eng. Technol*. 38 (2015) 311.